Kinetic Modeling of API Oxidation: 1. The AIBN/H$_2$O/CH$_3$OH Radical "Soup"

Alon Grinberg Dana[a,b], Haoyang Wu[a], Duminda S. Ranasinghe[a], Frank C. Pickard IV[c],
Geoffrey P. F. Wood[c], Todd Zelesky[c], Gregory W. Sluggett[c], Jason Mustakis[c], William H. Green[a,*]

[a]*Department of Chemical Engineering, Massachusetts Institute of Technology, Cambridge, MA 02139, United States*
[b]*Wolfson Department of Chemical Engineering, Technion – Israel Institute of Technology, Haifa 3200003, Israel*
[c]*Pfizer Global Research & Development, Groton Laboratories, Eastern Point Road, Groton, CT 06340, United States*

Abstract

Stress testing of active pharmaceutical ingredients (API) is an important tool used to gauge chemical stability and identify potential degradation products. While different flavors of API stress testing systems have been used in experimental investigations for decades, the detailed kinetics of such systems as well as the chemical composition of prominent reactive species, specifically reactive oxygen species, are unknown. As a first step toward understanding and modeling API oxidation in stress testing, we investigated a typical radical "soup" solution an API is subject to during stress testing. Here we applied ab-initio electronic structure calculations to automatically generate and refine a detailed chemical kinetics model, taking a fresh look at API oxidation. We generated a detailed kinetic model for a representative azobisisobutyronitrile (AIBN)/H$_2$O/CH$_3$OH stress-testing system with varied co-solvent ratio (50%/50% – 99.5%/0.5% vol. water/methanol) and for representative pH values (4–10) at 40 ℃ stirred and open to the atmosphere. At acidic conditions hydroxymethyl alkoxyl is the dominant alkoxyl radical, and at basic conditions, for most studied initial methanol concentrations, cyanoisopropyl alkoxyl becomes the dominant alkoxyl radical, albeit at an overall lower concentration. At acidic conditions the levels of cyanoisopropyl peroxyl, hydroxymethyl peroxyl, and hydroperoxyl radicals are relatively high and comparable, while at both neutral and basic pH conditions, superoxide becomes the prominent radical in the system. The present work reveals the prominent species in a common model API stress testing system at various co-solvent and pH conditions, sets the stage for an in-depth quantitative API kinetic study, and demonstrates usage of novel software tools for automated chemical kinetic model generation and ab-initio refinement.

Keywords: Drug stress test, chemical kinetic modeling, AIBN, API oxidation stress testing, radical oxidation

1. Introduction

Understanding the chemical stability of active pharmaceutical ingredient (API) molecules is of great importance, as it affects the quality, safety, robustness, and efficacy of a drug product.[1] Improving and

---

*Corresponding author
Email address: whgreen@mit.edu (William H. Green)

streamlining processes related to early identification of potential API degradation products are paramount to assure that drug quality and safety is retained over its shelf life. Since this information can significantly affect the product development strategy, it is crucial to be able to predict, as early as possible in the development process, what may happen to a given drug candidate during its shelf life and to understand impurity profiles.[2, 3]

Stress testing, often referred to as "forced degradation", is an important tool used to identify potential degradation products, establish degradation pathways, and confirm the stability-indicating power of the analytical method.[4] Three types of oxidative stress testing are commonly used: (1.) using hydrogen peroxide to cover nucleophilic-electrophilic (2-electron) oxidations, (2.) using azoalkanes to cover free-radical oxidation, and (3.) using transition metals to cover single electron transfer oxidations. It was previously shown that the reactivity and selectivity can be better controlled by using a radical initiator, such as 2,2'-Azobis(2-methylpropionitrile) (azobisisobutyronitrile, or AIBN), rather than using hydrogen peroxide [5] or through regulation of temperature and oxygen levels.[5, 6] A radical initiator can be used to generate known fluxes of peroxyl radicals since its decomposition rate is often known.[7, 8] While several azoalkanes are used for stress testing,[9] usage of AIBN as a radical initiator is relatively common. [9, 10, 11, 12, 13, 14, 15, 16]

Upon homolysis, AIBN, a symmetrical azo-compound, yields two cyanoisopropyl radicals which quickly produce cyanoisopropyl peroxyl radicals in the presence of molecular oxygen. Peroxyl radicals are considered the primary reactive oxygen species involved in free radical oxidative processes of an API. However, it was previously suggested that, in the absence of a substrate reactive towards peroxyl radicals, highly reactive byproduct alkoxyl radicals such as cyanoisopropyl alkoxyl are also formed in an AIBN system and may represent a significant source of the observed reactivity.[17, 15]

Only very rarely is it feasible to study reactions of known amounts of a single radical species with a specific, well-defined substrate. Even a "clean" source of peroxyl radicals, for example, introduces alkoxyl and carbon-centered radicals generated via dimerization and fragmentation reactions, and may result in data which can be difficult to decipher from a mechanistic point of view.[17] To try to control this problem, methanol is being introduced into the aqueous system as a co-solvent, since methanol is known to significantly quench the reactivity of alkoxyl radicals, allowing for more predictive API stress testing experiments.[15] Nonetheless, introducing methanol as a co-solvent into this already complex system affects the identity and concentration of species, and is currently not entirely understood. Moreover, the presence of methanol induces byproducts such as formaldehyde which was reported to facilitate the Strecker reaction (amine conversion into aminonitrile) in this system.[13]

A representative $AIBN/H_2O/CH_3OH$ stress-testing system is considered in the present work. The exact radical chemistry of this important system is complicated and not well understood. The current literature is unclear regarding which are the prominent radicals and what their concentrations are. To date, no thorough, quantitative kinetic study has been reported for this or any similar stress testing system.

Computational chemistry approaches could complement and assist experimental API stress-testing in var-

ious ways: (1.) visualizing and quantifying information regarding molecular structures, (2.) answering questions pertaining to reaction mechanisms, and (3.) honing questions that can be investigated experimentally.[9] Specifically, such tools can answer many important questions in the current system of interest. While pharmaceutical stress-testing beckons with many opportunities for applying computational chemistry, relatively little work has been published in this area.[9] Contemporary methods for drug degradation predictions (discussed elsewhere [18]) rely on a combination of *in-cerebo* and *in-silico* methods. Development of some previous drug degradation prediction software was discontinued primarily due to inflexibilities. Zeneth [19] is the only currently (commercially) available software designed to predict drug degradation pathways. Zeneth makes useful qualitative predictions based on experimentally-validated reaction templates, but it does not incorporate kinetics capabilities, nor does it make quantitative predictions.

This work is first in a series describing kinetic modeling of API oxidation. It sets the stage for quantitatively describing API degradation by first carefully examining the radical "soup," *i.e.*, identifying the chemical environment an API is subject to during stress testing. The goal of the present work is to quantitatively describe the kinetics of 5.0 mM AIBN in a water-methanol co-solvent system using computational approaches. The objectives are to suggest an elementary chemical reaction mechanism, to determine the relative concentrations and the identity of prominent radical species, and to determining the effect of both methanol concentration and pH on species concentrations.

An important aspect of this work is that the methodology makes use of cutting-edge automated tools for kinetic model generation and refinement, many of which were developed by some of the present authors. Consequently, this approach can now be readily applied to similar systems using the methods discussed herein.

2. Methods

2.1. Kinetic Modeling

2.1.1. Model Generation

The kinetic model reported in this work was generated using the open-source Reaction Mechanism Generator (RMG) software.[20, 21] RMG automatically explores possible intermediate species and elementary reactions for a given reacting mixture based on reaction families and libraries, primarily using a flux-based algorithm. The software uses experimental and calculated thermodynamic and rate coefficient parameters from its database, and where data is missing it is estimated.[20] It is extensively utilized for modeling various gas-phase reactive systems,[22, 23, 24, 25, 26, 27] and has liquid-phase capabilities,[28, 29] including an estimation scheme for temperature-dependent solvation effects on thermochemistry [30] and a diffusion-limited kinetics correction.[31, 32] While RMG applies solvent corrections to equilibrium constants and so reverse rates, it does not apply any solvent corrections to forward rate coefficients except for diffusion limits. Therefore the solvent corrections for important reactions in the present work were separately calculated using

COSMO-RS (TZVPD-Fine), and individually fed into the RMG database. The current version of RMG does not support ionic reactions, so those reactions were added manually to the kinetic model.

The model was generated for an initial mixture of 5.0 mM AIBN, 0.43 mM inert N_2, and 0.22 mM O_2 at 40 °C in a water/methanol solution with a varying co-solvent ratio. The model was generated for a solvent concentration ratio range of 50%/50% – 99.5%/0.5% vol. water/methanol (equivalent to 27.78 M/12.36 M – 55.28 M/0.12 M water/methanol). Henry's law for pure water as a solvent was used to estimate the solubility of N_2 and O_2 in the solution at the respective temperature.[33] The concentrations of N_2, O_2, OH^-, and H_3O^+ were held constant throughout all simulations to mimic a buffered system open to the atmosphere. The properties of water were used by RMG to estimate ΔG^*_{solv} for all species. The model generation was terminated after 72 hours of simulation time, a characteristic time for experimental stress testing. The tolerance to include species in the RMG model (called "tolerance move to core") was set to 0.1% of the characteristic rate.

The AIBN homolysis rate coefficient was obtained from a literature measurement of the evolved nitrogen gas at constant pressure at 90–107 °C,[7] and extrapolated to the relevant system temperature. The rate coefficient for hydroxymethyl radical recombination with O_2 forming methanol hydroperoxyl, $\cdot CH_2OH + O_2 \rightleftharpoons HOCH_2OO\cdot$, was taken from a literature CBS-QB3 level of theory calculation,[34] and the rate coefficient of formaldehyde condensation with water, $CH_2O + H_2O \rightleftharpoons HOCH_2OH$, was taken from an experimental measurement at 20–50 °C and a pH range of 5–7[35]. An experimental rate coefficient was used for hydroxymethyl hydroperoxide decomposition into formaldehyde and hydrogen peroxide, $HOCH_2OOH \rightleftharpoons CH_2O + H_2O_2$.[36] Rate coefficients of cyanoisopropyl peroxyl radical recombination into a tetroxide and its subsequent homolysis into two cyanoisopropyl alkoxyl radicals and O_2 were taken from a 298 K experimental study [37] and an average of recommended rates for a similar tert-alkyl system,[38] respectively. Additional liquid phase rate coefficients for radical recombination with molecular oxygen were taken from literature [39] and added as training reactions into RMG's database.

The gas phase rate coefficient of hydroxymethyl peroxyl radical homolysis, $HOCH_2OO\cdot \rightleftharpoons CH_2O + HO_2\cdot$, (Fig. S2) is about 300 s^{-1} at 40 °C,[40, 41, 42, 43] and hydroxymethyl peroxyl levels are known to be regulated by this homolysis [43] which typically dominates over hydrogen abstraction pathways from hydrocarbon substrates.[42] However, in aqueous phase the rate coefficient of its degradation is about an order of magnitude slower, determined experimentally to be lower than 10 s^{-1} at 22 °C.[44] This decrease in rate coefficient is reasonable, since the hydroxyl and peroxyl groups of the reactant are available to hydrogen-bond with the solvent matrix, but become unavailable in the transition state, resulting in a higher activation energy. Consequently, at relatively high hydroxymethyl peroxyl concentrations in aqueous phase, second-order recombination reactions become important.[45] The lifetime of the hydroxymethyl peroxyl radical has a strong pH dependence,[44, 46] primarily due to the reaction of this peroxyl radical with hydroxide anion, yielding superoxide anion: $OHCH_2OO + OH^- \rightleftharpoons CH_2O + H_2O + O_2^-\cdot$.

The rate coefficient for $O_2^- \cdot + H^+ \rightleftharpoons HO_2$ was taken from a review of $HO_2\cdot/O_2^- \cdot$ reactivity in

aqueous solutions.[47] Rate coefficients for superoxide conversion into hydroxide, $O_2^- \cdot + HO_2 + H_2O \rightleftharpoons H_2O_2 + O_2 + OH^-$ and $O_2^- \cdot + H_2O \rightleftharpoons OH^- + HO_2$, were taken from an experimental measurement.[48, 49] Note that while $ROO \cdot + O_2^- \cdot + H_2O \rightleftharpoons ROOOO^{-*} + H_2O \rightleftharpoons ROOH + O_2 + OH^-$ reactions where allowed in the model, reactions of the sort $ROO^- + O_2 + H_2O \rightleftharpoons ROOOO^{-*} + H_2O$ were not considered since they are spin-forbidden.

Additional rate coefficients were taken from four literature sources (small H/O species chemistry,[50] and C/H/O systems [51, 52, 53]) previously compiled into the RMG database. Care was taken in the present work to exclude from these sources exclusive gas-phase routes, such as well-skipping pressure-dependent pathways. Rate coefficients which were identified as important were computed by the authors, as discussed below, and are given in Tables S1–S3. Other rate coefficients (when not taken from literature nor calculated by the authors) were estimated by RMG's reaction family templates.

Thermodynamic properties of small hydrogen- and oxygen-containing species were taken from literature,[50] and properties for additional species were taken from computed entries previously entered into the RMG database (the "CBS QB3 1dHR", "thermo DFT CCSDTF12 BAC", and "DFT QCI thermo" RMG libraries). Thermodynamic properties for additional species were computed by the authors, as described below, and are given in Table S4. A ΔG^*_{solv} correction was added to all neutral species thermodynamic properties, regardless of their data source, using the Abraham model[54, 55] implemented in RMG.[56] Note that while RMG has mature thermodynamic property estimation schemes, species' thermodynamic properties in the final model were all either directly calculated or taken from literature sources.

Thermodynamic properties for a subset of species which includes all ions in the model (OH^-, H^+, $O_2^- \cdot$, $HO_2 \cdot$, H_2O_2, and H_2O) were determined carefully to obtain thermodynamic consistency with literature equilibrium constants (Table S5). A standard state of 1 M was used, and the ΔG^*_f of H^+ was set to zero as a convention. Standard enthalpies and entropies of formation for H_2O and H_2O_2 were taken from NIST Chemistry WebBook.[57] The standard enthalpy of formation for $HO_2 \cdot$ was taken from the Active Thermochemical Tables (ATcT) project,[58] while the respective standard entropy of formation was taken from NIST Chemistry WebBook[57] as well. Respective standard Gibbs free energies of solvation, ΔG^*_{solv}, were taken from literature.[59] The liquid phase Gibbs free energies of formation of OH^- and of $O_2^- \cdot$ were determined using the above values and along with the H_2O K_{eq} of 1.01E-14 and $HO_2 \cdot$ pKa of 4.88 [60] constraints.

2.1.2. Statistical Mechanics

Statistical mechanics computations were performed using the Automated Reaction Kinetics and Network Exploration (Arkane) software package, available as part of the Reaction Mechanism Generator (RMG) software suite. [20] Arkane uses the output of computations done via various electronic structure software, and reads in quantities such as the electronic energy, vibrational frequencies, and torsional scans. Partition function calculations are based on the rigid rotor harmonic oscillator (RRHO) approximation with hindered internal torsion corrections. Torsional modes are projected out from the calculated Hessian. When calculat-

ing thermochemical parameters, spin, atom energy, and bond additivity energy corrections are all applied to the electronic energy. Arkane uses transition state theory [61, 62] with an optional tunneling correction (the present study uses the Eckart potential [63]) to compute reaction rate coefficients.

2.1.3. Automation

Chemical kinetic mechanisms involving complex reactions of numerous intermediates often rely on first-principles calculations as the main source of thermodynamic and rate parameters, especially when the number of important reactions in the real system greatly exceeds the number of available experimental data.[22, 64] The Automated Rate Calculator (ARC) software [65] automates the process of calculating parameters relevant for chemical kinetic modeling. ARC uses the cheminformatics modules RDKit [66] and OpenBabel [67, 68] to generate random 3D coordinate conformer guesses for species from the respective 2D structure, and has a mapping algorithm to deduce likely lowest energy conformers. ARC harnesses users' existing electronic structure software and manages job submission to users' servers. In a normal workflow, ARC optimizes the geometries of a set of low energy derived conformers and selects the lowest energy one. It will then spawn single-point energy calculations as well as frequency and dihedral scan computations based on the identified lowest energy geometry. ARC has a collection of troubleshooting methods to automatically manage the computation directives sent to the electronic structure software in case these jobs fail to converge. Eventually, ARC calls a statistical mechanics and rate theory software, in this case Arkane, to transform the raw computations into data relevant for kinetics simulations: thermodynamic properties and reaction rate coefficients.

The process of model generation and refinement using first-principle calculations was automated using The Tandem Tool (T3) software,[69] which iteratively executes RMG and ARC. It identifies chemical species in the RMG model that require refinement based on user criteria (*e.g.*, species for which the observables are sensitive and their respective uncertainty in Gibbs free energy is relatively high). These species are then sent to ARC for computation, and the resulting properties are added to the designated species's thermodynamic library within the RMG database. The next RMG-generated model executed by T3 results in somewhat different species and reactions, since it is based on additional (refined) data. T3 iteratively repeats this process until it achieves convergence, defined as the state where no new species answer the refinement criteria. In the present work the kinetic model is relatively small, hence T3 was set to refine all species participating in the model if their respective thermodynamic properties were based on an estimation.

2.1.4. Model Simulation

The model was simulated using the Reaction Mechanism Simulator (RMS) software,[70] which was used for computing species concentration profiles as well as rate of production. Absolute and relative tolerances of 10^{-20} and 10^{-10}, respectively, were used in the simulation.

6

2.2. Quantum Mechanical Calculations

2.2.1. Molecular Characterization

Kinetic parameters were calculated at the DLPNO-CCSD(T)/Def2-TZVP//ωB97X-D/Def2-TZVP level of theory (Tables S1–S3).[71, 72, 73] The Gaussian 16 electronic structure software package [74] was used for all DFT computations, and the Orca 4.2.1 electronic structure package [75] was used for the DLPNO-CCSD(T) single-point energy calculation with UHF and "tightPNO" parameters. A frequency scaling factor of 0.988, calculated in this work using methods described elsewhere,[76] was used when employing the ωB97X-D/Def2-TZVP method. The same DFT level was used for scanning torsional modes. Hindered rotor calculations were performed for each rotatable single bond, and each was treated as an independent rotor where 45 consecutive constrained optimizations with 8° increments were carried out per torsional mode. Relevant calculations were also added to the RMG database for the benefit of future users.

Initial guesses for transition state (TS) geometry optimizations were derived manually, and attempts to achieve lower TS conformers were made using functionalities implemented in ARC [65] in combination with Psi4,[77] an electronic structure software. ARC carried out the transition state optimization, along with frequency and single point energy calculation, and executed intrinsic reaction coordinate calculations to follow the reaction path to verify whether each transition state indeed corresponds to the correct reactants and products. A multi-structure approach was taken when computing rate coefficients. All 3D structures of species and transition states are available in the Supporting Information.

Thermodynamic parameters were computed at the CBS-QB3 level of theory [78, 79] (Table S4) using the Gaussian 16 electronic structure software package.[74] Geometry optimization and frequency calculations in the CBS-QB3 method were performed at the B3LYP/CBSB7 level of theory,[78, 80] and a frequency scaling factor of 1.004 [76] was used.

2.2.2. Solvation Corrections

Solvent effects upon kinetic parameters were modeled using the COSMO-RS solvation energy correction [81] using a 50%/50% vol. water/methanol solution as the solvent using a TZVPD-fine level. Thermochemical parameters were automatically corrected by RMG, as mentioned above. Charge surfaces for the COSMO-RS calculation were calculated using Turbomole 7.4.0 [82] based on the gas-phase geometry as determined at the ωB97X-D/Def2-TZVP level of theory. We also performed gas-phase single-point energy calculations at BVP86/TZVPD-Fine/DGA1,[83, 84, 85, 86] using Turbomole 7.4.0. Both the COSMO result file (".cosmo") and the gas phase energy file (".energy") generated by Turbomole 7.4.0 were used in the COSMOtherm 2020 [87] software to compute the free energy of solvation. This procedure was carried out for reactants, products, and transition states. The solvent correction term was added to the gas-phase single-point energy value.

3. Results and Discussion

3.1. Quantum Mechanical Computation Results

Rate coefficients of $RO\cdot + CH_3OH \rightleftharpoons \cdot CH_2OH + ROH$ and $ROO\cdot + CH_3OH \rightleftharpoons \cdot CH_2OH + ROOH$ for major alkoxyl ($RO\cdot$) and peroxyl ($ROO\cdot$) radicals in the reactive mixture (where R equals $OHCH_2$ or cyanoisopropyl) were computed using the methods detailed above. Rate coefficients associated with alkoxyl radicals were found to be significantly faster than those involving peroxyl radicals, revealing the strong reactivity of alkoxyl radicals (Figure 1). Our results are in agreement with literature findings where alkoxyl radicals were shown to react 5–7 orders of magnitude faster than analogous peroxyl radicals via hydrogen abstraction reactions.[11] Additional calculated rate coefficients are summarized in the Supporting Information (Table S1).
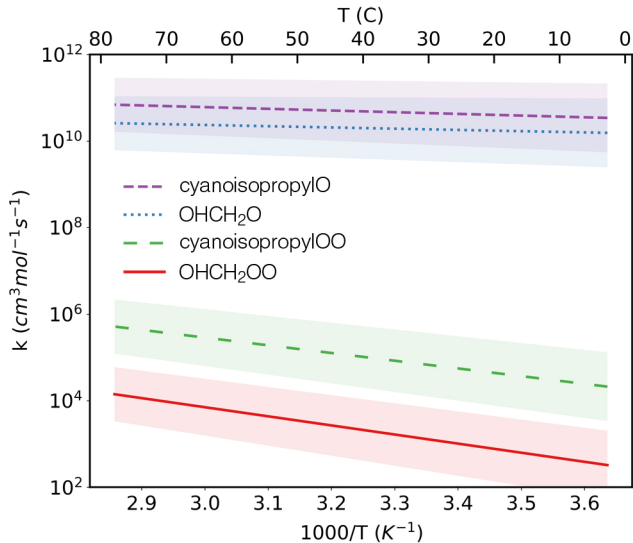

Figure 1: Rate coefficients of hydrogen abstraction from the methyl group of methanol by major alkoxyl and peroxyl radicals in the system. Shaded areas represent the rate uncertainty from propagating a 1 kcal mol^{-1} uncertainty from the computed activation energy.

The rate coefficients of hydrogen abstraction by these alkoxyl and peroxyl radicals from the hydroxyl group of methanol, i.e., $RO\cdot + CH_3OH \rightleftharpoons CH_3O\cdot + ROH$ and $ROO\cdot + CH_3OH \rightleftharpoons CH_3O\cdot + ROOH$, were also calculated. In agreement with literature hydrogen abstraction rate coefficients for other abstracting radicals,[88] abstracting hydrogen from the hydroxyl group (Fig. S1) is significantly slower compared to abstracting a hydrogen atom from the methyl group of methanol (Fig. 1).

3.2. Modeling

The model generated in the present work consists of 27 chemical species and 94 elementary reactions. During the model generation process, more than 200 species and nearly 1500 reactions were automatically explored by RMG. The model (forward rate coefficients and thermodynamic properties) is provided in the

Supporting Information in a machine and human readable format (YAML) as well as in a more human friendly format in Tables S6–S8.

The initial methanol concentration effect on the concentration of various species in this system at 72 hours can be seen in Figure 2 for three representative pH values. As intended in this system,[15] an increase in the initial methanol concentration causes a significant decrease in the concentration of cyanoisopropyl alkoxyl radical at all pH values. The initial methanol concentration has a lesser effect on the other alkoxyl radicals in this system, hydroxymethyl alkoxyl ($HOCH_2O\cdot$) and hydroperoxymethoxyl ($.OCH_2OOH$) radicals.

Stable end products (acetone, hydrogen cyanide, hydrogen peroxide, formic acid, and formaldehyde) present only a small pH or initial methanol concentration dependency in the entire studied range. Furthermore, the concentrations of both cyanoisopropyl peroxyl and cyanoisopropyl alkoxyl radicals are nearly agnostic to the pH level as well. The pH level naturally has a direct affect over AH/A^- ratios such as $HO_2\cdot/O_2-\cdot$, as well as an indirect effect over the absolute levels of $HO_2\cdot$ and $O_2-\cdot$. The levels of all non-nitrogenous alkoxyl radicals, as well as hydroxymethyl peroxyl radical, all decrease with increasing pH values.

As a result of a combined initial methanol concentration and pH value effects, and since hydroxymethyl alkoxyl is just as undesired for drug stress testing as cyanoisopropyl alkoxyl radical is, increasing the methanol concentration at acidic or neutral pH has but a weak effect over the total alkoxyl radical concentration in the system. On the other hand, at basic conditions cyanoisopropyl alkoxyl is the prominent alkoxyl radical at a most of the studied initial methanol level range, and at pH 10, increasing the methanol concentration is only effective in quenching alkoxyl radicals (directly or indirectly) up to about 8 M (equivalent to about 30% vol.), where their absolute level is already low relative to respective lower pH conditions.

The pH value affects the concentration of hydroxymethyl peroxyl, but not the concentration of cyanoisopropyl peroxyl radical. At pH 4 and a relatively high methanol concentration the levels of these peroxyl radicals as well as hydroperoxyl are comparable and they are the prominent radicals in the system. As the pH value increases, the levels of superoxide radical ($O_2-\cdot$) become more significant, and at neutral and basic conditions it is the dominant radical in the system. At pH 10 and high initial methanol levels the concentration of superoxide is about three orders of magnitude higher than the next prominent radical at these conditions, cyanoisopropyl peroxyl. A similar phenomenon, where the pH value affects the levels of hydroxymethyl alkoxyl radical but not the levels of cyanoisopropyl alkoxyl radicals, can be observed (Fig. 2). At acidic conditions, hydroxymethyl alkoxyl is the dominant alkoxyl radical, and as the pH increases its levels decrease, resulting in a shift of the dominant alkoxyl radical in the system that depends on the initial methanol levels. At pH 10, cyanoisopropyl alkoxyl becomes the dominant alkoxyl radical at most of the studied initial methanol concentration range, and the levels of these two alkoxyl radicals become nearly equivalent at the high methanol concentration regime. The overall peroxyl radical concentration remains similar at different pH values since it is masked by the relatively high cyanoisopropyl peroxyl radical level which is pH-agnostic, while the overall alkoxyl radical concentration decreases with increasing pH levels.

9

Reaction flux diagrams at 24 hours for three representative pH values of 4, 7, and 10 (Figs. 3–5) portray dominant reaction pathways in this system. The nitrogen transformation route, starting with AIBN homolysis, passing through four cyanoisopropyl species and ending in equimolar amounts of hydrogen cyanide and acetone is principally similar at all studied pH values. The major difference is that at basic pH the radical termination reaction, cyanoisopropylOO + O_2^- + H_2O $\rightleftharpoons$ cyanoisopropylOOH + O_2 + OH^-, becomes relatively significant due to the increasing concentration of superoxide. The insensitivity of the nitrogen transformation route to the pH level can also be seen by the pH-agnostic characteristic of both cyanoisopropyl peroxyl and cyanoisopropyl alkoxyl radicals (Fig. 2 A–C). On the other hand, the relative importance of other pathways stemming from methanol and hydroxymethyl radical vary significantly with pH.

At acidic conditions (Fig. 3), the hydroxide-assisted decomposition of hydroxymethyl peroxyl radical is relatively slow, resulting in a relatively long lifetime of this radical. Consequently, the concentration of hydroxymethyl peroxyl is relatively high (Fig. 2 A) and therefore its reaction rates of self recombination, homolysis, hydrogen abstraction from methanol, and reaction with superoxide are all relatively significant (Fig. 3). At neutral and basic conditions (Figs. 4, 5), the base-catalyzed decomposition rate of hydroxymethyl peroxyl radical forming formaldehyde and superoxide radical dominates over reaction rates of competing decomposition pathways, resulting in a relatively short lifetime and a lower concentration of the hydroxymethyl peroxyl radical (Fig. 2). As the pH level increase, accompanied by a decrease in the concentration of hydroxymethyl peroxyl, the levels of superoxide, the product of this base-catalyzed decomposition, increase.

While the cyanoisopropyl peroxyl radical level is strongly affected by the initial methanol concentration, the hydroxymethyl peroxyl radical level is nearly agnostic to the initial methanol concentration at the studied conditions (Fig 2). The formation rate of the cyanoisopropyl peroxyl radical is independent of the methanol concentration, while its consumption rate does depend on the methanol levels: either directly or indirectly when mediated via superoxide (Fig. 5). On the other hand, the reactivity of hydroxymethyl peroxyl radicals is characterized by an interesting chain reaction. Hydroxymethyl peroxyl radicals react with methanol to form $\cdot CH_2OH$ radicals that recombine with molecular oxygen to give more hydroxymethyl peroxyl radicals. Alternatively, hydroxymethyl peroxyl radicals can decompose via a base-catalyzed reaction yielding superoxide radicals which are in equilibrium with hydroperoxyl radicals that also contribute to methanol conversion into $\cdot CH_2OH$, yielding more hydroxymethyl peroxyl radicals as well (Fig. 4). The former applies to all pH values, while the latter chain reaction is most prominent at neutral pH where the levels of hydroxymethyl peroxyl radicals are not too high to mask this pathway (as occurs at acidic conditions), and the level of hydroperoxyl radicals is not too low (as occurs basic conditions).

Formaldehyde reacts with hydrogen peroxide or water, yielding formic acid and methylene glycol as end products of the methanol oxidation branch. Interestingly, no alkoxyl radicals are significantly involved in the major pathways at these conditions, suggesting that methanol does not directly quench alkoxyl radicals in this system in a significant manner, but rather prevents their formation in the first place by reacting with the cyanoisopropyl peroxyl precursor, lowering its self-recombination rate. Superoxide self recombination

rate is known to be slow,[89] and its loss mechanism in this system is mainly via hydronium cation, forming its acid counterpart hydroperoxyl radical. The high levels of superoxide in this system may have important implications toward the reactivity of API molecules in stress testing, and should be considered in future mechanisms explaining API oxidation pathways since its reactivity differs than the reactivity of carbon-center peroxyl radicals.

At lower methanol concentrations radical recombination reactions become more significant: important pathways include hydroxymethyl peroxyl radical self-recombination pathways and cyanoisopropyl peroxyl radical self-recombination, the later mainly forms two cyanoisopropyl alkoxyl radicals. At low methanol concentrations, hydrogen radical generation is relatively significant, stemming from a β-scission reaction of the hydroxymethyl alkoxyl radical. This β-scission reaction is only slightly endothermic ($\sim$ 2 kcal mol^{-1}); the alternative β-scission reaction of hydroxymethyl alkoxyl radical forming formaldehyde and hydroxyl radical is significantly more endothermic ($\sim$ 23 kcal mol^{-1}) and it rate is insignificant in this system.

Speciation time-profiles at neutral pH and at two extreme methanol concentration cases, 50% and 0.05% vol., are given in Figs. 6 and S3, respectively. Cyanoisopropyl peroxide is the first non-radical species in the nitrogen transformation route other than the radical initiator. It is therefore the only non-radical species that reaches a quasi-steady state within a relatively short time (nearly instantaneously compared to the experiment time). The system is accumulating end products (e.g., acetone and hydrogen cyanide), while most reactive oxygen species reach a quasi-steady state nearly instantaneously. For a given solvent composition and pH value, the system is mostly well-defined with near-constant levels of many reactive species.

The concentration of hydrogen cyanide, a side-product generated from cyanoisopropyl alcohol hydrolysis (Figs. 3–5), is not significantly affected by the added methanol. At basic pH, hydrogen cyanide (pK_a = 9.4 [90]) is converted into cyanide anion, which is believed to contribute, along with formaldehyde, to artifact generation in the degradation products of APIs.[13] Cyanide anion facilitates the Strecker reaction, which yields α-aminonitrile, containing primary or secondary amine motifs. At the conditions studied here, the concentration of hydrogen cyanide reaches $\sim$ 1 mM (Fig. 6). The conversion (i.e., reacted vs. initial amount) of AIBN during the studies 72-hour period is about 10%–11%.

Only the concentration of superoxide significantly increases with increasing pH values, other than trivially the levels of hydroxyl anion (Fig. 7). Increasing the pH value has a significant effect over the levels of alkoxyl radicals, decreasing the concentration of hydroxymethyl alkoxyl by seven orders of magnitude between pH 4 and 10. On the other hand, increasing the pH also decreases the level of cyanoisopropyl peroxyl radical, by nearly three orders of magnitude at the same pH range.

A sensitivity analysis was conducted for major radicals in this system with regard to all reaction rate coefficients (Figs. 8, S4–S6). The goal of sensitivity analysis is twofold: It assists is assessing the effect of model parameters on the observables and hence the propagation of uncertainties, and it gives insights onto the system's dynamics. Here we present the top five reaction rate coefficients to which an observable is

sensitive. The normalized sensitivity coefficients for superoxide (Fig. 8 A) were found to be relatively small in magnitude, and superoxide was found to be most sensitive to the rate coefficients of AIBN homolysis and hydroperoxyl recombination. Both rate coefficients were taken from experimental studies performed at different conditions: one using xylene as the solvent[7] and the other in gas phase[91], respectively. To improve the superoxide concentration predictions of the present model, these two rate coefficients should be determined more precisely at more relevant conditions. Nonetheless, the experimental literature sources provide reasonable values even in the present context, and the relatively small normalized sensitivity coefficients of superoxide implies relatively low uncertainties in the present prediction of superoxide levels.

The normalized sensitivity coefficients for hydroxymethyl alkoxyl (Fig. 8 B) are relatively large in magnitude, implying that the uncertainty in the prediction of the levels of this alkoxyl radical could be relatively large. However, since the absolute levels of hydroxymethyl alkoxyl are small to begin with (Figs 2, 6, 7), the propagated uncertainty should not be significant in absolute terms. The levels of hydroxymethyl alkoxyl are sensitive to the AIBN homolysis rate coefficient which largely dictates the concentration of all radicals in the system. The levels of hydroxymethyl alkoxyl are also sensitive to the rate coefficient of the base-catalyzed hydroxymethyl peroxyl radical decomposition into formaldehyde, yet only at relatively early times. This reaction indeed consumes hydroxymethyl peroxyl, the precursor of hydroxymethyl alkoxyl, and therefore the respective normalized sensitivity coefficient is negative. The time dependency of these sensitivity coefficients could be understood in light of the chain reaction discussed above: after a short initialization period in which the concentration of hydroxymethyl peroxyl radicals stabilize (Fig. 6), consumption of hydroxymethyl peroxyl radicals enhances their formation via hydrogen abstraction reactions from methanol, thus stabilizing the system. This stabilization is expressed as a decrease in the absolute value of the normalized sensitivity coefficients of both hydroxymethyl peroxyl (Fig. S4) and hydroxymethyl alkoxyl (Fig. 8 B) radicals to the rate coefficients of the main hydroxymethyl peroxyl consumption channel and of the AIBN homolysis reaction.

4. Conclusion

To facilitate chemical stability studies of API molecules, a detailed chemical kinetic model of the stress testing system itself (the "soup") was generated. The computationally studied system consists of 5.0 mM AIBN in a water-methanol solution at varied co-solvents ratio at 40 °C and varied pH values open to the atmosphere.

After 72 hours at 40 °C the conversion of AIBN was about 10%–11%. The identity and concentration of the most prominent radicals in this system vary with conditions. At acidic conditions cyanoisopropyl peroxyl, hydroxymethyl peroxyl, and hydroperoxyl are the prominent radicals. This picture changes as pH values increase. At neutral conditions superoxide is predicted to be the most prominent radical, and its concentration significantly increases at basic conditions. At acidic conditions hydroxymethyl alkoxyl is the dominant alkoxyl radical, and at basic conditions cyanoisopropyl alkoxyl becomes the dominant alkoxyl rad-

ical at most initial methanol concentrations, albeit at a lower overall concentration. Increasing the methanol concentration at acidic or neutral pH has only a weak effect over the total alkoxyl radical concentration in the system. On the other hand, at basic conditions increasing the methanol concentration is effective in quenching alkoxyl radicals (directly or indirectly), yet only up to about 8 M (equivalent to about 30% vol.)

No alkoxyl radicals are significantly involved in the major pathways at the studied conditions, suggesting that methanol does not directly quench alkoxyl radicals in this system significantly, but rather prevents their formation in the first place by reacting with the peroxyl radical precursors. The nitrogen transformation route, passing through different cyanoisopropyl species, is mostly insensitive to the pH value.

The reactivity of methanol radicals depend on the pH value. At acidic and neutral pH, where the base-catalyzed decomposition of hydroxymethyl peroxyl radicals is not too fast, this radical reacts with methanol, forming a chain reaction which sustains its concentration. Consequently, the level of hydroxymethyl peroxyl radicals do not significantly depend on the initial methanol concentration throughout at these conditions. At acidic pH, where the rate of this base-catalyzed reaction is relatively slow, a variety of competing hydroxymethyl peroxyl radical decomposition pathways reactions become significant.

This study sheds light on the AIBN/water/methanol system and its elementary kinetic mechanism at various conditions. It also shows the feasibility and potential of harnessing computational chemistry and automated kinetic model generation and refinement schemes to low temperature liquid-phase systems.

This work is first in a series of detailed kinetic modeling of API oxidation, and sets the stage for quantitatively describing API degradation by first carefully examining the radical "soup," *i.e.*, identifying the chemical environment an API is subject to during stress testing. The model was generated using automated software tools, some of which were very recently developed and are described here for the first time. While more work is necessary in this field, e.g., representing pH-dependent reaction rates and determining the explicit solvent effect on reaction transition states, this work represents both a significant advancement in understanding a typical system in which API molecules undergo oxidation, as well as a substantial progress in automated computational tools for studying reactive chemical systems in general.

5. Acknowledgments

6. Supporting Information

Figure S1: Rate coefficients of hydrogen radical abstraction from the hydroxyl group of methanol by major alkoxyl and peroxyl radicals in the system.

Figure S2: Rate coefficients of the gas-phase dissociation reaction OHCH2OO<=>CH2O+HO2.

Figure S3: Selected species concentrations vs. time at pH 7 and 0.05% vol. methanol.

Figure S4: Sensitivity analysis of hydroxymethyl peroxyl radical to reaction rate coefficients.

Figure S5: Sensitivity analysis of cyanoisopropyl peroxyl radical to reaction rate coefficients.

Figure S6: Sensitivity analysis of cyanoisopropyl alkoxyl radical to reaction rate coefficients.

Table S1: Calculated reaction rate coefficients that were used in the model, accounting for solvation effect on the standard Gibbs energy and for tunneling

Table S2: Calculated reaction rate coefficients, accounting for solvation effect on the standard Gibbs energy but not for tunneling (showing the effect of tunneling over the rate)

Table S3: Calculated reaction rate coefficients, not accounting for solvation effect on the standard Gibbs energy but accounting for tunneling (showing the solvation effect over the rate)

Table S4: Calculated gas-phase thermodynamic parameters at the CBS-QB3 level of theory

Table S5: Determined aqueous-phase thermodynamic parameters

Table S6: Reaction rate coefficients in the model

Table S7: Species thermodynamic parameters in the model

Table S8: Species structures

The kinetic model used in this work in an RMS YAML format.

All transition state Cartesian 3D geometries are given.

TOC image:

References

[1] S. Yoshioka, V. J. Stella, Stability of drugs and dosage forms, Springer Science & Business Media, 2000.

[2] M. Blessy, R. D. Patel, P. N. Prajapati, Y. Agrawal, Development of forced degradation and stability indicating studies of drugs—a review, Journal of Pharmaceutical Analysis 4 (3) (2014) 159 – 165. `doi:10.1016/j.jpha.2013.09.003`.

[3] C. Gressl, M. Brunsteiner, A. Davis, M. Landis, K. Pencheva, G. Scrivens, G. W. Sluggett, G. P. F. Wood, H. Gruber-Woelfler, J. G. Khinast, A. Paudel, Drug–excipient interactions in the solid state: The role of different stress factors, Molecular Pharmaceutics 14 (12) (2017) 4560–4571. `doi:10.1021/acs.molpharmaceut.7b00677`.

[4] ICH Q1A(R2) stability testing of new drugs substances and products, ICH steering committee (2003).

[5] B. Giovanni, C. Deleuze, M. Gachon, G. Palmisano, J. P. Vergnaud, Autoxidation of tetrazepam in tablets: Prediction of degradation impurities from the oxidative behavior in solution, Journal of Pharmaceutical Sciences 81 (2) (1992) 183 – 185. `doi:10.1002/jps.2600810216`.

[6] G. Boccardi, Autoxidation of drugs: Prediction of degradation impurities from results of reaction with radical chain initiators, Farmaco (Societa chimica italiana : 1989) 49 (6) (1994) 431—435.
URL `http://europepmc.org/abstract/MED/7915522`

[7] R.-S. Juang, J.-F. Liang, Thermal decomposition of azobisisobutyronitrile dissolved in xylene in the presence of tin(iv) chloride, Journal of Chemical Technology and Biotechnology 55 (4) (1992) 379–383. `doi:10.1002/jctb.280550413`.

[8] R. T. Dean, J. V. Hunt, A. J. Grant, Y. Yamamoto, E. Niki, Free radical damage to proteins: The influence of the relative localization of radical generation, antioxidants, and target proteins, Free Radical Biology and Medicine 11 (2) (1991) 161 – 168. `doi:10.1016/0891-5849(91)90167-2`.

[9] S. W. Baertschi, K. M. Alsante, R. A. Reed, Pharmaceutical stress testing: Predicting drug degradation, CRC Press, 2016.

[10] S. W. Baertschi, K. M. Alsante, et al., Stress testing: the chemistry of drug degradation, in: Pharmaceutical stress testing, CRC Press, 2016, pp. 61–153.

[11] M. A. Watkins, S. Pitzenberger, P. A. Harmon, Direct evidence of 2-cyano-2-propoxy radical activity during aibn-based oxidative stress testing in acetonitrile–water solvent systems, Journal of Pharmaceutical Sciences 102 (5) (2013) 1554 – 1568. `doi:10.1002/jps.23500`.

[12] D. W. Reynolds, M. Galvani, S. R. Hicks, B. J. Joshi, S. A. Kennedy-Gabb, M. H. Kleinman, P. Z. Parmar, The use of n-methylpyrrolidone as a cosolvent and oxidant in pharmaceutical stress testing, Journal of Pharmaceutical Sciences 101 (2) (2012) 761 – 776. `doi:10.1002/jps.22793`.

[13] M. Nefliu, T. Zelesky, P. Jansen, G. W. Sluggett, C. Foti, S. W. Baertschi, P. A. Harmon, Artifacts generated during azoalkane peroxy radical oxidative stress testing of pharmaceuticals containing primary and secondary amines, Journal of Pharmaceutical Sciences 104 (12) (2015) 4287 – 4298. `doi:10.1002/jps.24667`.

[14] N. Haman, E. Longo, A. Schiraldi, M. Scampicchio, Radical scavenging activity of lipophilic antioxidants and extra-virgin olive oil by isothermal calorimetry, Thermochimica Acta 658 (2017) 1 – 6. `doi:10.1016/j.tca.2017.10.012`.

[15] E. D. Nelson, G. M. Thompson, Y. Yao, H. M. Flanagan, P. A. Harmon, Solvent effects on the aibn forced degradation of cumene: Implications for forced degradation practices, Journal of Pharmaceutical Sciences 98 (3) (2009) 959 – 969. `doi:10.1002/jps.21489`.

[16] M. Davies, R. Dean, Radical-mediated Protein Oxidation: From Chemistry to Medicine, Oxford science publications, Oxford University Press, 1997.
URL https://books.google.com/books?id=TIWNQgAACAAJ

[17] M. J. Davies, R. T. Dean, Radical-Mediated Protein Oxidation: From Chemistry to Medicine, Oxford University Press, 1999. doi:10.1146/10.1086/393060.

[18] C. Foti, K. Alsante, G. Cheng, T. Zelesky, M. Zell, Tools and workflow for structure elucidation of drug degradation products, TrAC Trends in Analytical Chemistry 49 (2013) 89 – 99. doi:10.1016/j.trac.2013.06.005.

[19] A. D. Parenty, W. G. Button, M. A. Ott, An expert system to predict the forced degradation of organic molecules, Molecular pharmaceutics 10 (8) (2013) 2962–2974. doi:10.1021/mp400083h.

[20] C. W. Gao, J. W. Allen, W. H. Green, R. H. West, Reaction mechanism generator: Automatic construction of chemical kinetic mechanisms, Computer Physics Communications 203 (2016) 212–225. doi:10.1016/j.cpc.2016.02.013.

[21] M. Liu, A. G. Dana, M. Johnson, M. Goldman, A. Jocher, A. M. Payne, C. Grambow, K. Han, N. W.-W. Yee, E. Mazeau, K. Blondal, R. West, F. Goldsmith, W. H. Green, Reaction Mechanism Generator v3.0: Advances in Automatic Mechanism Generation, Journal of Chemical Information and Modelingdoi:10.26434/chemrxiv.13489656.v1.

[22] W. H. Green, Chapter 5 - automatic generation of reaction mechanisms, Computer Aided Chemical Engineering 45 (2019) 259–294. doi:10.1016/B978-0-444-64087-1.00005-X.

[23] S. V. Petway, H. Ismail, W. H. Green, E. G. Estupiñán, L. E. Jusinski, C. A. Taatjes, Measurements and automated mechanism generation modeling of oh production in photolytically initiated oxidation of the neopentyl radical, J. Phys. Chem. A 111 (2007) 3891–3900. doi:10.1021/jp0668549.

[24] M. R. Harper, K. M. V. Geem, S. P.Pyl, G. B.Marin, W. H.Green, Comprehensive reaction mechanism for n-butanol pyrolysis and combustion, Combustion and Flame 158 (2011) 16–41. doi:10.1016/j.combustflame.2010.06.002.

[25] A. G. Dana, B. Buesser, S. Merchant, W. Green, Automated reaction mechanism generation including nitrogen as a heteroatom, Int. J. Chem. Kin. 50 (2018) 243–258. doi:10.1002/kin.21154.

[26] T.-C. Chu, Z. J. Buras, P. Oßwald, M. Liu, M. J. Goldman, W. H. Green, Modeling of aromatics formation in fuel-rich methane oxy-combustion with an automatically generated pressure-dependent mechanism, Phys. Chem. Chem. Phys. 21 (2019) 813–832. doi:10.1039/C8CP06097E.

[27] L. Lai, H.-W. Pang, W. H. Green, Formation of two-ring aromatics in hexylbenzene pyrolysis, Energy & Fuels 34 (2) (2020) 1365–1377. doi:10.1021/acs.energyfuels.9b03223.

16

[28] D. C. Mielczarek, M. Matrat, A. B. Amara, Y. Bouyou, P. Wund, L. Starck, Toward the accurate prediction of liquid phase oxidation of aromatics: A detailed kinetic mechanism for toluene autoxidation, Energy & Fuels 31 (11) (2017) 12893–12913. `doi:10.1021/acs.energyfuels.7b00416`.

[29] K. Chatelain, A. Nicolle, A. Ben Amara, L. Starck, L. Catoire, Structure–reactivity relationships in fuel stability: Experimental and kinetic modeling study of isoparaffin autoxidation, Energy & Fuels 32 (9) (2018) 9415–9426. `doi:10.1021/acs.energyfuels.8b01379`.

[30] Y. Chung, R. J. Gillis, W. H. Green, Temperature-dependent vapor–liquid equilibria and solvation free energy estimation from minimal data, AIChE Journal 66 (6) (2020) e16976. `doi:10.1002/aic.16976`.

[31] S. A. Rice, Diffusion-limited reactions, Elsevier, 1985.

[32] M. B. Flegg, Smoluchowski reaction kinetics for reactions of any order, SIAM Journal on Applied Mathematics 76 (4) (2016) 1403–1432. `doi:10.1137/15M1030509`.

[33] S. Sander, J. Abbatt, J. Barker, J. Burkholder, R. Friedl, D. Golden, R. Huie, M. Kurylo, G. Moortgat, V. Orkin, P. Wine, Chemical kinetics and photochemical data for use in atmospheric studies, evaluation no. 17, jpl publication 10-6, jet propulsion laboratory, pasadena, us (2011).
URL `http://jpldataeval.jpl.nasa.gov`

[34] T. S. Dibble, Mechanism and dynamics of the ch2oh+o2 reaction, Chemical Physics Letters 355 (1) (2002) 193 – 200. `doi:10.1016/S0009-2614(02)00211-7`.

[35] J. Winkelman, O. Voorwinde, M. Ottens, A. Beenackers, L. Janssen, Kinetics and chemical equilibrium of the hydration of formaldehyde, Chemical Engineering Science 57 (19) (2002) 4067 – 4076. `doi:10.1016/S0009-2509(02)00358-5`.

[36] Z. Xianliang, Y. Lee, Aqueous solubility and reaction kinetics of hydroxymethyl hydroperoxide, The Journal of Physical Chemistry 1 (1992) 265–272.
URL `https://pubs.acs.org/doi/pdf/10.1021/j100180a051`

[37] T. G. Denisova, V. F. Shuvalov, Recombination of 1,1-dimethylpropyl peroxy radicals in polar solvents, Kinetics and Catalysis 57 (1) (2016) 22 – 25. `doi:10.1134/S0023158416010031`.

[38] S. L. Khursan, Organic tetroxides and mechanism of peroxy radical recombination, American Cancer Society, 2014, pp. 1, 34. `doi:10.1002/9780470682531.pat0827`.

[39] P. Neta, R. E. Huie, A. B. Ross, Rate constants for reactions of peroxyl radicals in fluid solutions, Journal of Physical and Chemical Reference Data 19 (2) (1990) 413–513. `doi:10.1063/1.555854`.

[40] I. Barnes, K. Becker, E. Fink, A. Reimer, F. Zabel, H. Niki, Ftir spectroscopic study of the gas-phase reaction of ho2 with h2co, Chemical Physics Letters 115 (1) (1985) 1–8.

[41] B. Veyret, R. Lesclaux, M. Rayez, J. Rayez, R. Cox, G. Moortgat, Kinetics and mechanism of the photo-oxidation of formaldehyde. 1. flash photolysis study, The Journal of Physical Chemistry 93 (6) (1989) 2368–2374.

[42] I. Hermans, J.-F. Müller, T. L. Nguyen, P. A. Jacobs, J. Peeters, Kinetics of α-hydroxy-alkylperoxyl radicals in oxidation processes. ho2-initiated oxidation of ketones/aldehydes near the tropopause, The Journal of Physical Chemistry A 109 (19) (2005) 4303–4311, pMID: 16833760. `doi:10.1021/jp044080v`.

[43] P. Morajkar, C. Schoemaecker, M. Okumura, C. Fittschen, Direct measurement of the equilibrium constants of the reaction of formaldehyde and acetaldehyde with ho2 radicals, International Journal of Chemical Kinetics 46 (5) (2014) 245–259.

[44] E. Bothe, G. Behrens, D. Schulte-Frohlinde, Mechanism of the first order decay of 2-hydroxy-propyl-2-peroxyl radicals and of o2 formation in aqueous solution, Zeitschrift für Naturforschung B 32 (8) (1977) 886 – 889. `doi:10.1515/znb-1977-0811`.

[45] R. E. Huie, C. L. Clifton, Kinetics of the self-reaction of hydroxymethylperoxyl radicals, Chemical Physics Letters 205 (2) (1993) 163 – 167. `doi:10.1016/0009-2614(93)89222-4`.

[46] J. Rabani, D. Klug-Roth, A. Henglein, Pulse radiolytic investigations of ohch2o2 radicals, The Journal of Physical Chemistry 78 (21) (1974) 2089–2093.

[47] B. H. J. Bielski, D. E. Cabelli, R. L. Arudi, A. B. Ross, Reactivity of ho_2/o_2^- radicals in aqueous solution, Journal of Physical and Chemical Reference Data 14 (4) (1985) 1041–1100. `doi:10.1063/1.555739`.

[48] B. H. J. Bielski, Reevaluation of the spectral and kinetic properties of ho2 and o2- free radicals, Photochemistry and Photobiology 28 (4-5) (1978) 645–649. `doi:10.1111/j.1751-1097.1978.tb06986.x`.

[49] M. Mohammad, A. Y. Khan, M. S. Subhani, N. Bibi, S. Ahmad, S. Saleemi, Kinetics and electrochemical studies on superoxide, Research on Chemical Intermediates 27 (3) (2001) 259–267. `doi:10.1163/156856701300356473`.

[50] M. P. Burke, M. Chaos, Y. Ju, F. L. Dryer, S. J. Klippenstein, Comprehensive h2/o2 kinetic model for high-pressure combustion, International Journal of Chemical Kinetics 44 (7) (2012) 444–474. `doi:10.1002/kin.20603`.

[51] H. Hashemi, J. M. Christensen, S. Gersen, H. Levinsky, S. J. Klippenstein, P. Glarborg, High-pressure oxidation of methane, Combustion and Flame 172 (2016) 349 – 364. `doi:10.1016/j.combustflame.2016.07.016`.

[52] P. Glarborg, J. A. Miller, B. Ruscic, S. J. Klippenstein, Modeling nitrogen chemistry in combustion, Progress in Energy and Combustion Science 67 (2018) 31 – 68. `doi:10.1016/j.pecs.2018.01.002`.

[53] J. Bugler, B. Marks, O. Mathieu, R. Archuleta, A. Camou, C. Grégoire, K. A. Heufer, E. L. Petersen, H. J. Curran, An ignition delay time and chemical kinetic modeling study of the pentane isomers, Combustion and Flame 163 (2016) 138 – 156. `doi:10.1016/j.combustflame.2015.09.014`.

[54] M. Vitha, P. W. Carr, The chemical interpretation and practice of linear solvation energy relationships in chromatography, Journal of Chromatography A 1126 (1) (2006) 143 – 194, the Role of Theory in Chromatography. `doi:10.1016/j.chroma.2006.06.074`.

[55] M. H. Abraham, J. A. Platts, A. Hersey, A. J. Leo, R. W. Taft, Correlation and estimation of gas–chloroform and water–chloroform partition coefficients by a linear free energy relationship method, Journal of Pharmaceutical Sciences 88 (7) (1999) 670–679. `doi:10.1021/js990008a`.

[56] A. Jalan, R. W. Ashcraft, R. H. West, W. H. Green, Predicting solvation energies for kinetic modeling, Annu. Rep. Prog. Chem., Sect. C: Phys. Chem. 106 (2010) 211–258. `doi:10.1039/B811056P`.

[57] Nist chemistry webbook, nist standard reference database number 69 (2018). `doi:10.18434/T4D303`.

[58] B. Ruscic, R. E. Pinzon, G. von Laszewski, D. Kodeboyina, A. Burcat, D. Leahy, D. Montoy, A. F. Wagner, Active thermochemical tables: thermochemistry for the 21st century, Journal of Physics: Conference Series 16 (2005) 561–570. `doi:10.1088/1742-6596/16/1/078`.

[59] C. P. Kelly, C. J. Cramer, D. G. Truhlar, Aqueous solvation free energies of ions and ion-water clusters based on an accurate value for the absolute aqueous solvation free energy of the proton, The Journal of Physical Chemistry B 110 (32) (2006) 16066–16081, pMID: 16898764. `doi:10.1021/jp063552y`.

[60] D. Behar, G. Czapski, J. Rabani, L. M. Dorfman, H. A. Schwarz, Acid dissociation constant and decay kinetics of the perhydroxyl radical, The Journal of Physical Chemistry 74 (17) (1970) 3209–3213. `doi:10.1021/j100711a009`.

[61] D. G. Truhlar, W. L. Hase, J. T. Hynes, Current status of transition-state theory, The Journal of Physical Chemistry 87 (15) (1983) 2664–2682. `doi:10.1021/j100238a003`.

[62] D. G. Truhlar, B. C. Garrett, S. J. Klippenstein, Current status of transition-state theory, The Journal of Physical Chemistry 100 (31) (1996) 12771–12800. `doi:10.1021/jp953748q`.

[63] H. S. Johnston, J. Heicklen, Tunnelling corrections for unsymmetrical eckart potential energy barriers, The Journal of Physical Chemistry 66 (3) (1962) 532–533. `doi:10.1021/j100809a040`.

[64] W. H. Green, Moving from postdictive to predictive kinetics in reaction engineering, AIChE Journal 66 (11) (2020) e17059. `doi:10.1002/aic.17059`.

[65] A. G. Dana, D. Ranasinghe, H. Wu, C. Grambow, X. Dong, M. Johnson, M. Goldman, M. Liu, W. H. Green, ARC - automated rate calculator (2020). `doi:10.5281/zenodo.3356849`.

[66] RDKit: Cheminformatics and Machine Learning Software; http://www.rdkit.org.

[67] N. M. O'Boyle, M. Banck, C. A. James, C. Morley, T. V. . G. R. Hutchison, Open babel: An open chemical toolbox, Journal of Cheminformatics 3. `doi:10.1186/1758-2946-3-33`.

[68] The Open Babel Package, version 2.3.1 http://openbabel.org.

[69] A. G. Dana, K. Spiekermann, W. Green, The tandem tool (T3) for automated kinetic model generation and refinement. https://github.com/reactionmechanismgenerator/t3, version 0.1.0, `https://github.com/ReactionMechanismGenerator/T3` (2020).

[70] M. Johnson, W. Green, Rms - reaction mechanism simulator. https://github.com/reactionmechanismgenerator/reactionmechanismsimulator.jl, version 0.1.0, `https://github.com/ReactionMechanismGenerator/ReactionMechanismSimulator.jl` (2020).

[71] C. Riplinger, P. Pinski, U. Becker, E. F. Valeev, F. Neese, Sparse maps - A systematic infrastructure for reduced-scaling electronic structure methods. II. Linear scaling domain based pair natural orbital coupled cluster theory, Journal of Chemical Physics 144 (2) (2016) 024109. `doi:10.1063/1.4939030`.

[72] F. Weigend, R. Ahlrichs, Balanced basis sets of split valence, triple zeta valence and quadruple zeta valence quality for H to Rn: Design and assessment of accuracy, Physical Chemistry Chemical Physics 7 (18) (2005) 3297–3305. `doi:10.1039/b508541a`.

[73] J. D. Chai, M. Head-Gordon, Long-range corrected hybrid density functionals with damped atom-atom dispersion corrections, Physical Chemistry Chemical Physics 10 (44) (2008) 6615–6620. `doi:10.1039/b810189b`.

[74] M. J. Frisch, G. W. Trucks, H. B. Schlegel, G. E. Scuseria, M. A. Robb, J. R. Cheeseman, G. Scalmani, V. Barone, G. A. Petersson, H. Nakatsuji, X. Li, M. Caricato, A. V. Marenich, J. Bloino, B. G. Janesko, R. Gomperts, B. Mennucci, H. P. Hratchian, J. V. Ortiz, A. F. Izmaylov, J. L. Sonnenberg, D. Williams-Young, F. Ding, F. Lipparini, F. Egidi, J. Goings, B. Peng, A. Petrone, T. Henderson, D. Ranasinghe, V. G. Zakrzewski, J. Gao, N. Rega, G. Zheng, W. Liang, M. Hada, M. Ehara, K. Toyota, R. Fukuda, J. Hasegawa, M. Ishida, T. Nakajima, Y. Honda, O. Kitao, H. Nakai, T. Vreven, K. Throssell, J. A. Montgomery, Jr., J. E. Peralta, F. Ogliaro, M. J. Bearpark, J. J. Heyd, E. N. Brothers, K. N. Kudin, V. N. Staroverov, T. A. Keith, R. Kobayashi, J. Normand, K. Raghavachari, A. P. Rendell, J. C. Burant, S. S. Iyengar, J. Tomasi, M. Cossi, J. M. Millam, M. Klene, C. Adamo, R. Cammi, J. W. Ochterski, R. L. Martin, K. Morokuma, O. Farkas, J. B. Foresman, D. J. Fox, Gaussian~16 Revision C.01, gaussian Inc. Wallingford CT (2016).

[75] F. Neese, Software update: the orca program system, version 4.0, WIREs Computational Molecular Science 8 (1) (2018) e1327. `doi:10.1002/wcms.1327`.

[76] I. M. Alecu, J. Zheng, Y. Zhao, D. G. Truhlar, Computational thermochemistry: Scale factor databases and scale factors for vibrational frequencies obtained from electronic model chemistries, Journal of Chemical Theory and Computation 6 (9) (2010) 2872–2887. `doi:10.1021/ct100326h`.

[77] R. M. Parrish, L. A. Burns, D. G. A. Smith, A. C. Simmonett, A. E. DePrince, E. G. Hohenstein, U. Bozkaya, A. Y. Sokolov, R. Di Remigio, R. M. Richard, J. F. Gonthier, A. M. James, H. R. McAlexander, A. Kumar, M. Saitow, X. Wang, B. P. Pritchard, P. Verma, H. F. Schaefer, K. Patkowski, R. A. King, E. F. Valeev, F. A. Evangelista, J. M. Turney, T. D. Crawford, C. D. Sherrill, Psi4 1.1: An open-source electronic structure program emphasizing automation, advanced libraries, and interoperability, Journal of Chemical Theory and Computation 13 (7) (2017) 3185–3197, pMID: 28489372. `doi:10.1021/acs.jctc.7b00174`.

[78] J. A. Montgomery, M. J. Frisch, J. W. Ochterski, G. A. Petersson, A complete basis set model chemistry. vi. use of density functional geometries and frequencies, The Journal of Chemical Physics 110 (6) (1999) 2822–2827. `doi:10.1063/1.477924`.

[79] G. P. F. Wood, L. Radom, G. A. Petersson, E. C. Barnes, M. J. Frisch, J. A. Montgomery, A restricted-open-shell complete-basis-set model chemistry, The Journal of Chemical Physics 125 (9) (2006) 094106. `doi:10.1063/1.2335438`.

[80] A. D. Becke, Density-functional thermochemistry. iii. the role of exact exchange, The Journal of Chemical Physics 98 (7) (1993) 5648–5652. `doi:10.1063/1.464913`.

[81] F. Eckert, A. Klamt, Fast solvent screening via quantum chemistry: COSMO-RS approach, AIChE Journal 48 (2) (2002) 369–385. `doi:10.1002/aic.690480220`.

[82] S. G. Balasubramani, G. P. Chen, S. Coriani, M. Diedenhofen, M. S. Frank, Y. J. Franzke, F. Furche, R. Grotjahn, M. E. Harding, C. Hättig, A. Hellweg, B. Helmich-Paris, C. Holzer, U. Huniar, M. Kaupp, A. Marefat Khah, S. Karbalaei Khani, T. Müller, F. Mack, B. D. Nguyen, S. M. Parker, E. Perlt, D. Rappoport, K. Reiter, S. Roy, M. Rückert, G. Schmitz, M. Sierka, E. Tapavicza, D. P. Tew, C. v. Wüllen, V. K. Voora, F. Weigend, A. Wodyński, J. M. Yu, Turbomole: Modular program suite for ab initio quantum-chemical and condensed-matter simulations, The journal of chemical physics 152 (18) (2020) Article: 184107. `doi:10.1063/5.0004635`.

[83] A. D. Becke, Density-functional exchange-energy approximation with correct asymptotic behavior, Physical Review A 38 (6) (1988) 3098–3100. `doi:10.1103/PhysRevA.38.3098`.

[84] J. P. Perdew, Density-functional approximation for the correlation energy of the inhomogeneous electron gas, Physical Review B 33 (12) (1986) 8822–8824. `doi:10.1103/PhysRevB.33.8822`.

[85] A. Schäfer, C. Huber, R. Ahlrichs, Fully optimized contracted Gaussian basis sets of triple zeta valence quality for atoms Li to Kr, The Journal of Chemical Physics 100 (8) (1994) 5829–5835. `doi:10.1063/1.467146`.

660 [86] N. Godbout, D. R. Salahub, J. Andzelm, E. Wimmer, Optimization of gaussian-type basis sets for local spin density functional calculations. part i. boron through neon, optimization technique and validation, Canadian Journal of Chemistry 70 (2) (1992) 560–571. `doi:10.1139/v92-079`.

[87] COSMOtherm.
URL `http://www.cosmologic.de`

665 [88] I. M. Alecu, D. G. Truhlar, Computational study of the reactions of methanol with the hydroperoxyl and methyl radicals. 2. accurate thermal rate constants, The Journal of Physical Chemistry A 115 (51) (2011) 14599–14611, pMID: 22059377. `doi:10.1021/jp209029p`.

[89] B. H. J. Bielski, A. O. Allen, Mechanism of the disproportionation of superoxide radicals, The Journal of Physical Chemistry 81 (11) (1977) 1048–1050. `doi:10.1021/j100526a005`.

670 [90] D. Ripin, D. Evans, pka's of inorganic and oxo-acids (2005).
URL `http://ccc.chem.pitt.edu/wipf/MechOMs/evans_pKa_table.pdf`

[91] H. Hippler, J. Troe, J. Willner, Shock wave study of the reaction ho2+ho2→h2o2+o2 : Confirmation of a rate constant minimum near 700 k, The Journal of Chemical Physics 93 (3) (1990) 1755–1760. `doi:10.1063/1.459102`.
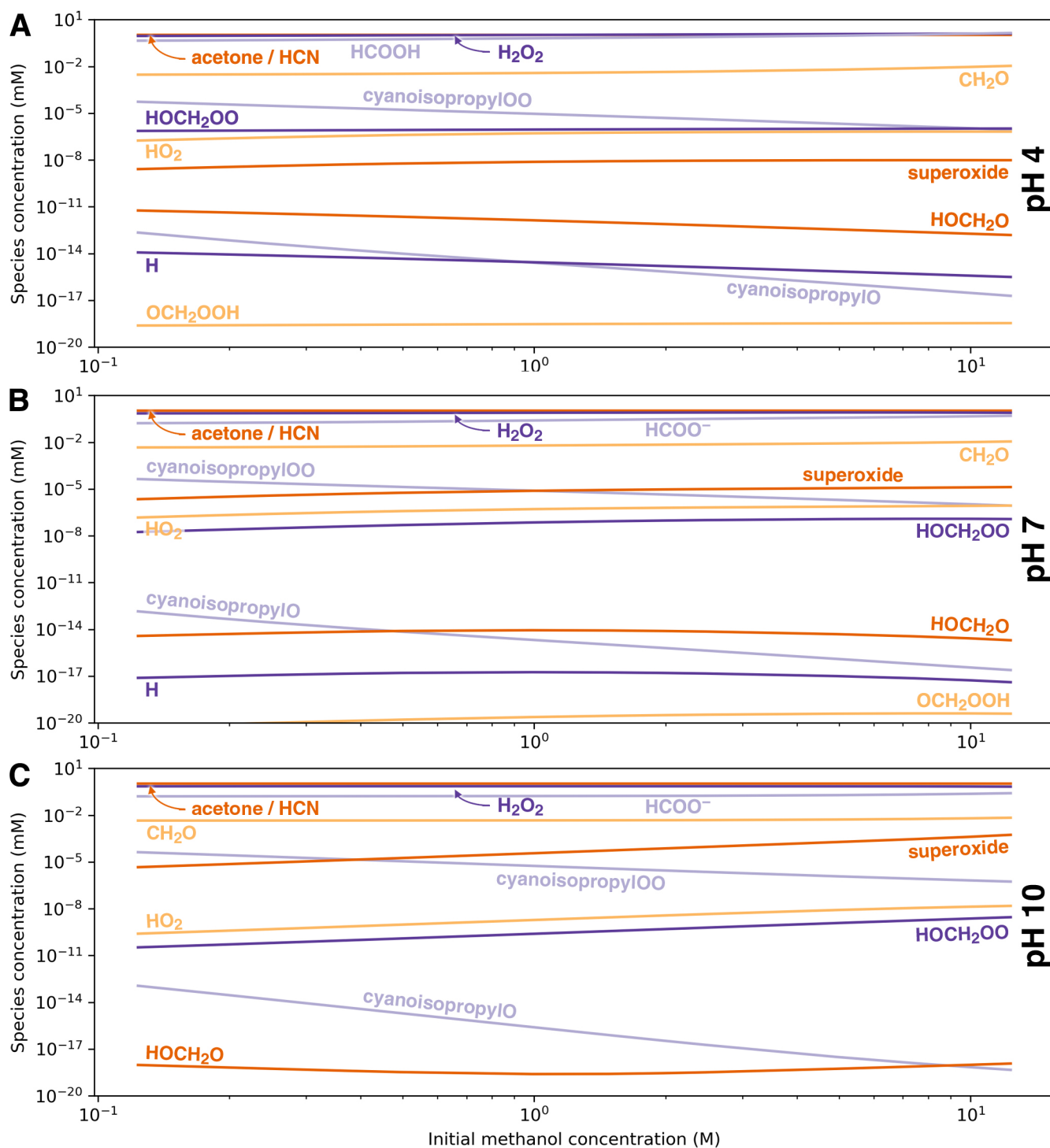
Figure 2: Selected species concentrations at 72 hours, 40 °C in a 5.0 mM AIBN methanol/water/O_2/N_2 system open to the atmosphere vs. the initial methanol concentration at pH values of (A) 4, (B) 7, and (C) 10. Note that the concentration trends of hydrogen cyanide and acetone are identical, and both are represented by a single line.
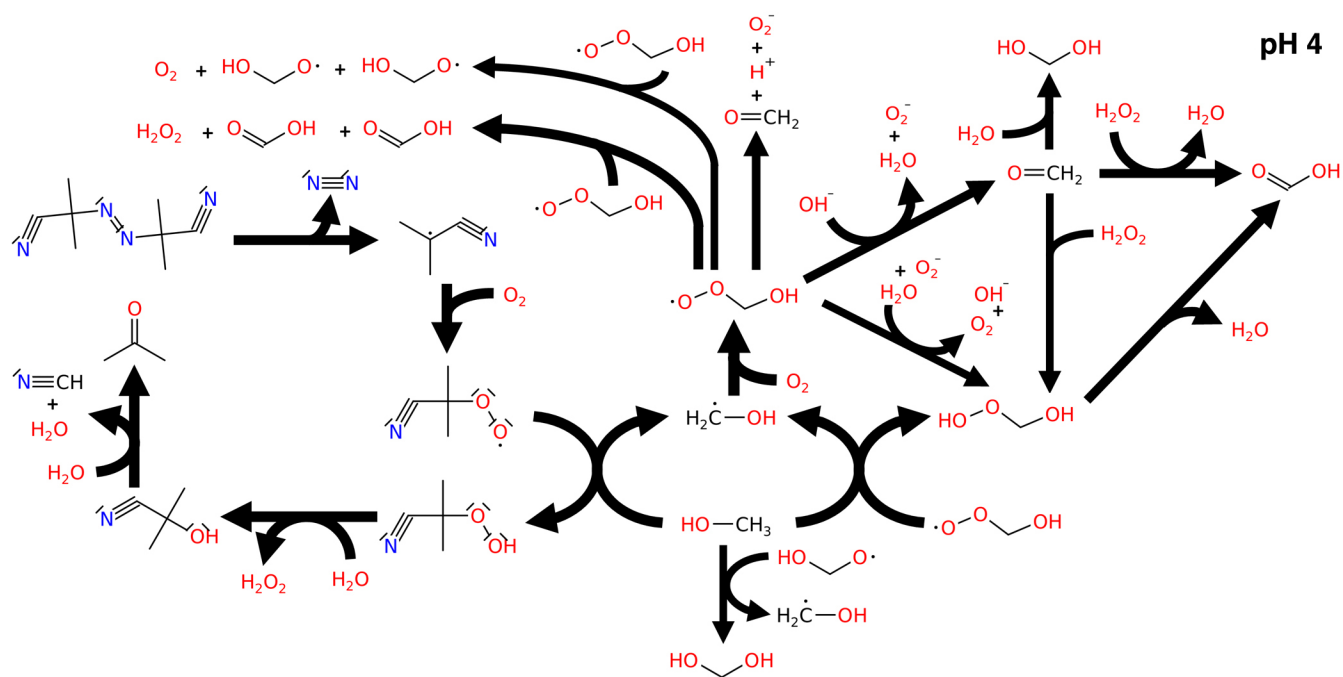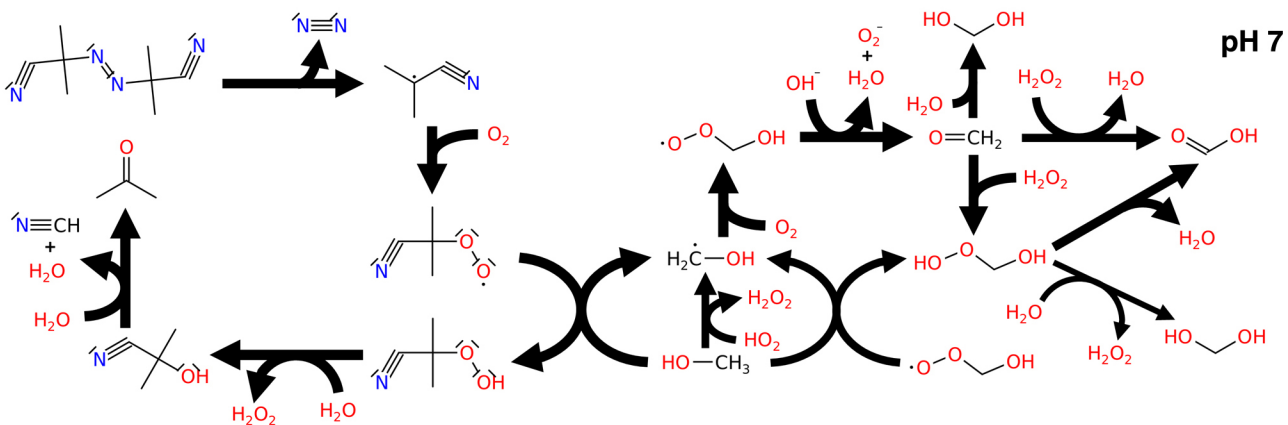
Figure 3: Major reaction pathways in the 5.0 mM AIBN methanol/water/O_2/N_2 system at 24 hours, 40 °C with solvent concentrations of 50%/50% vol. at pH 4. Branching ratios of hydroxymethyl peroxyl radical are important at low [OH^-]. Arrow widths correspond logarithmically to the respective net reaction rates. The diagram captures at least 95% of each species consumption rate; species with a total consumption rate < 10% of their respective total production rate were not explored further.
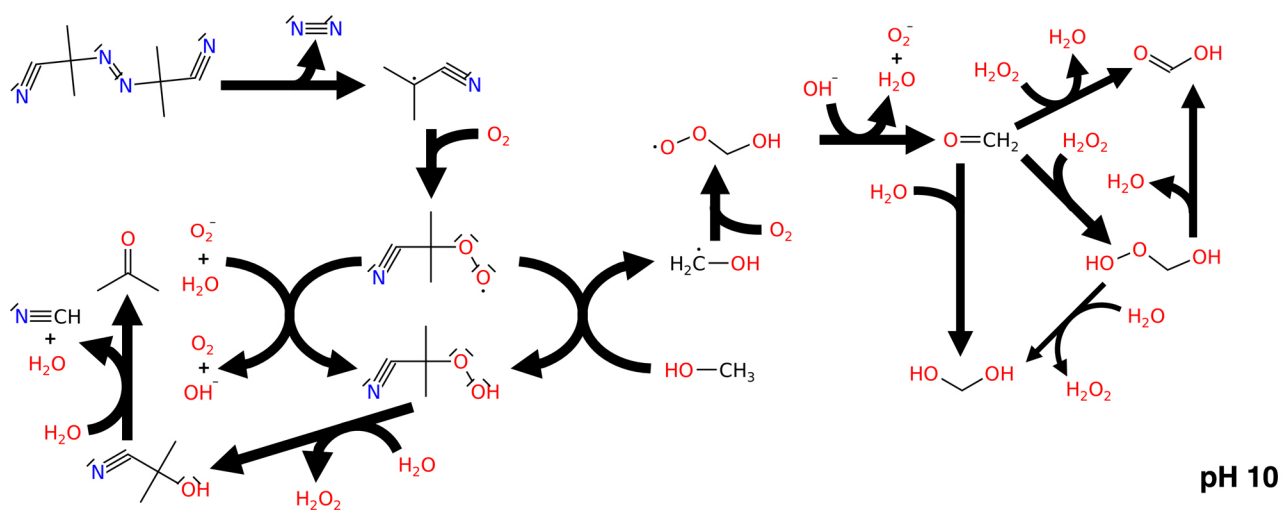

Figure 4: Major reaction pathways in the 5.0 mM AIBN methanol/water/O_2/N_2 system at 24 hours, 40 °C with solvent concentrations of 50%/50% vol. at pH 7. Hydroxymethyl peroxyl radical decomposition is base-catalyzed. Arrow widths correspond logarithmically to the respective net reaction rates. The diagram captures at least 95% of each species consumption rate; species with a total consumption rate < 10% of their respective total production rate were not explored further.

24

Figure 5: Major reaction pathways in the 5.0 mM AIBN methanol/water/O_2/N_2 system at 24 hours, 40 °C with solvent concentrations of 50%/50% vol. at pH 10. Levels of superoxide radical are significant and it participates in the nitrogen transformation route, partly replaces methanol. Arrow widths correspond logarithmically to the respective net reaction rates. The diagram captures at least 95% of each species consumption rate; species with a total consumption rate $< 10\%$ of their respective total production rate were not explored further.
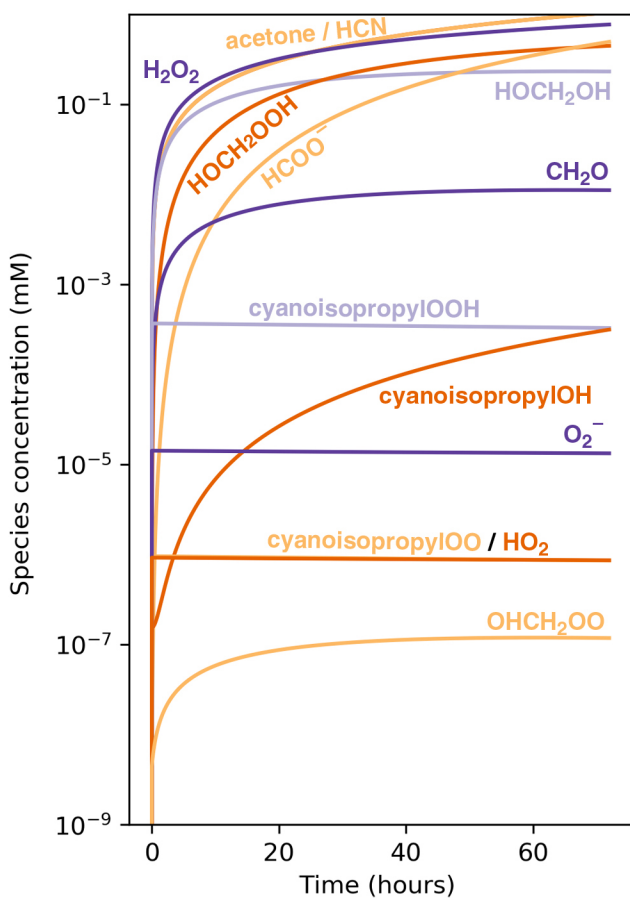
Figure 6: Selected species concentrations vs. time in the 5.0 mM AIBN methanol/water/O_2/N_2 system open to the atmosphere at 40 °C and pH 7. Solvent concentrations of 27.78 M/12.36 M water/methanol (equivalent to 50%/50% vol.).
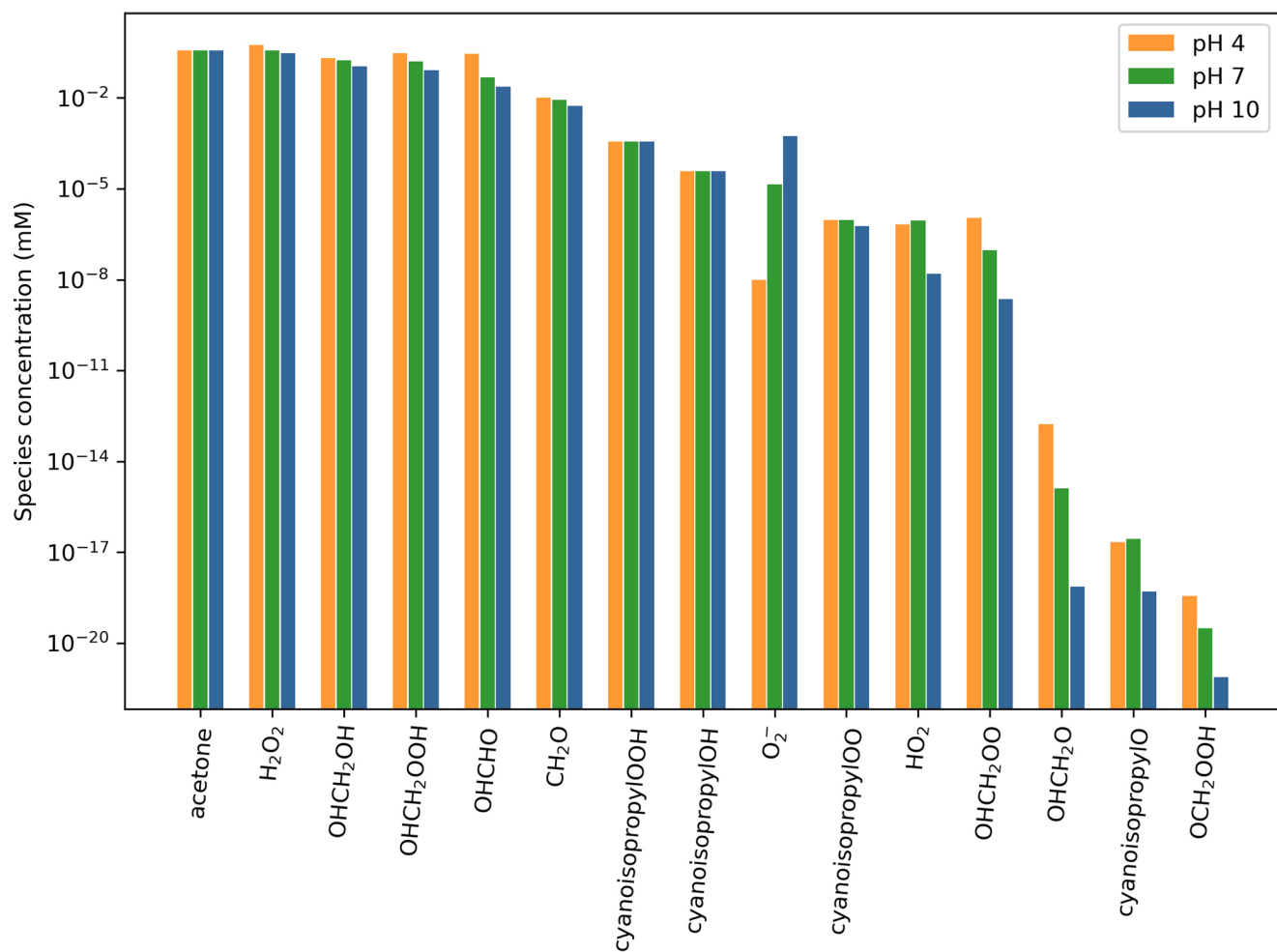
Figure 7: Selected species concentrations at three representative pH values in the 5.0 mM AIBN methanol/water/O_2/N_2 system open to the atmosphere at 40 °C at 24 hours. Solvent concentrations of 27.78 M/12.36 M water/methanol (equivalent to 50%/50% vol.). Hydrogen cyanide is not shown, its concentration is equal to that of acetone.
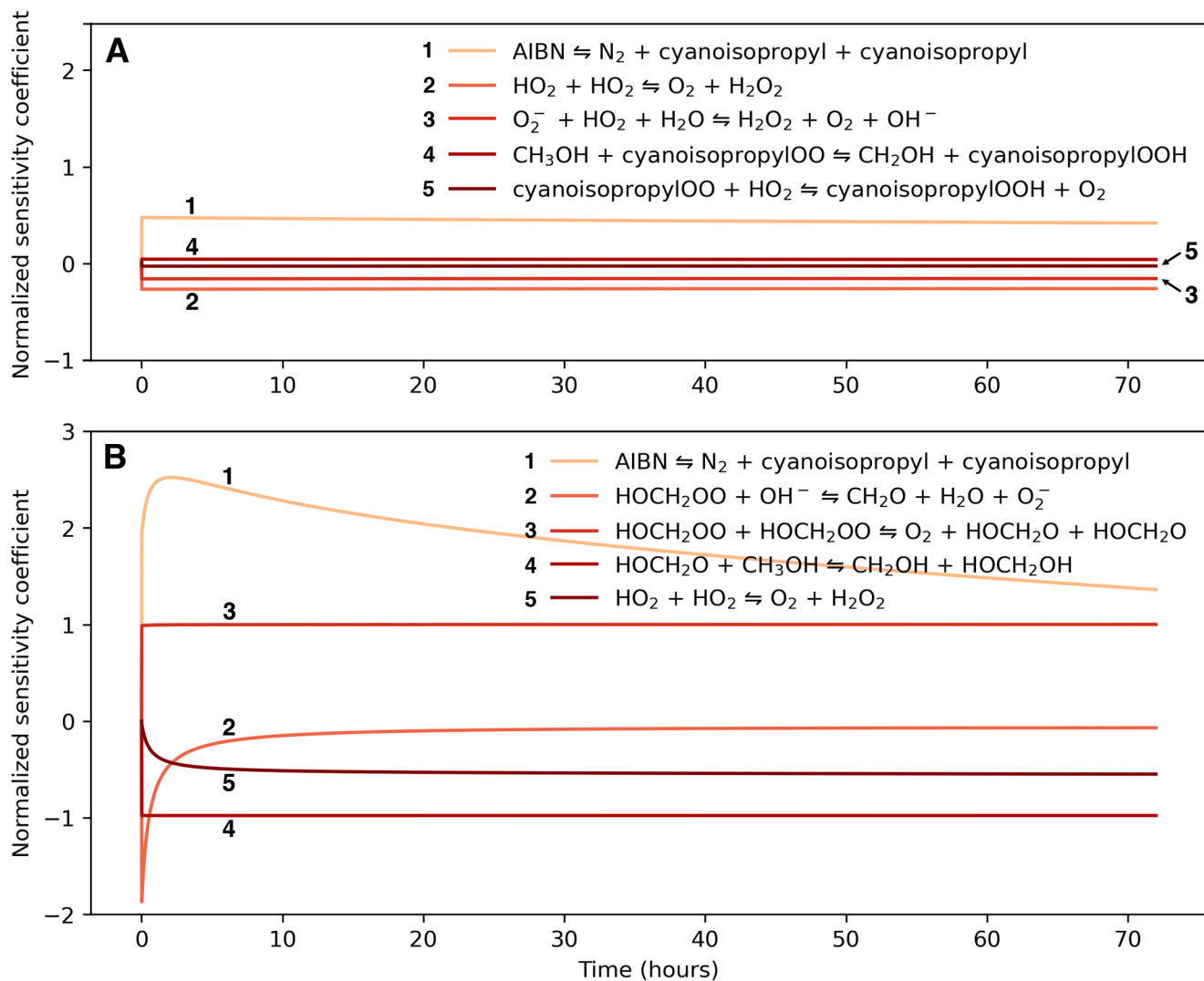
Figure 8: Sensitivity analysis, $\partial \ln [X]/\partial \ln k_i$, of (A) super oxide radical and (B) hydroxymethyl alkoxyl radical to reaction rate coefficients, showing the five reactions with the highest absolute normalized sensitivity coefficient. Computed for the 5.0 mM AIBN methanol/water/O_2/N_2 system open to the atmosphere at 40 °C at pH 7. Solvent concentrations are 27.78 M/12.36 M water/methanol (equivalent to 50%/50% vol.).
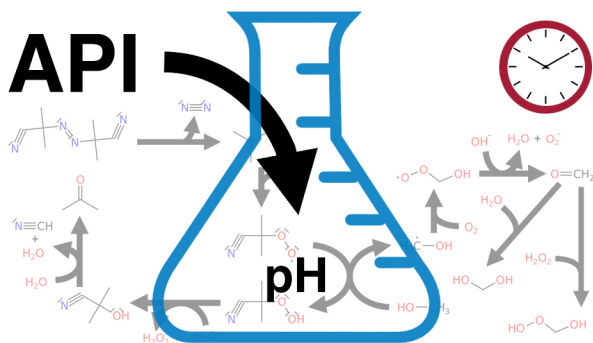

Figure 9: TOC image